Bio 3D Conduits Derived from Bone Marrow Stromal Cells Promote Peripheral Nerve Regeneration

Hirofumi Yurie[1], Ryosuke Ikeguchi[1] ©, Tomoki Aoyama[1], Mai Tanaka[1], Hiroki Oda[1], Hisataka Takeuchi[1], Sadaki Mitsuzawa[1] ©, Maki Ando[1], Koichi Yoshimoto[1], Takashi Noguchi[1], Shizuka Akieda[2], Koichi Nakayama[3] ©, and Shuichi Matsuda[1]

Abstract

We previously reported that a nerve conduit created from fibroblasts promotes nerve regeneration in a rat sciatic nerve model. This study aims to determine whether a nerve conduit created from bone marrow stromal cells (BMSCs) can promote nerve regeneration. Primary BMSCs were isolated from femur bone marrow of two Lewis rats, and cells at passages 4–7 were used. We created seven Bio 3D nerve conduits from BMSCs using a Bio-3D Printer. The conduits were transplanted to other Lewis rats to bridge 5-mm right sciatic nerve gaps (Bio 3D group, $n = 7$). We created two control groups: a silicone group (S group, $n = 5$) in which the same nerve gap was bridged with a silicone tube, and a silicone cell group (SC group, $n = 5$) in which the gap was bridged with a BMSC injection. Twelve weeks after transplantation, nerve regeneration was evaluated functionally and morphologically. In addition, PKH26-labeled BMSCs were used to fabricate a Bio 3D conduit that was transplanted for cell trafficking analysis. Electrophysiological study, kinematic analysis, wet muscle weight, and morphological parameters showed significantly better nerve regeneration in the Bio 3D group than in the S group or SC group. In immunohistochemical studies, sections from the Bio 3D group contained abundant S-100-positive cells. In cell trafficking analysis, PKH26-positive cells stained positive for the Schwann cell markers S-100, p75NTR, and GFAP. Bio 3D nerve conduits created from BMSCs can promote peripheral nerve regeneration in a rat sciatic nerve model through BMSC differentiation into Schwann-like cells.

Keywords

peripheral nerve, nerve regeneration, bone marrow stromal cells, nerve conduit, bio 3D printer

Introduction

Previously, we created a scaffold-free nerve conduit from fibroblast cells using a Bio-3D printer and reported that it promoted peripheral nerve regeneration in a rat sciatic nerve model[1,2]. This conduit was made from cells only and included no artificial scaffold[3–7]. Its advantages include lower risks of foreign material reaction and infection, and increased elasticity due to transplantation across joints[3–7].

Bone marrow stromal cells (BMSCs) are reported to have potential for peripheral nerve regeneration and differentiation into Schwann-like cells[8–10]. Previously, we have used fibroblasts for this purpose because fibroblasts are easy to culture and proliferate *in vitro*[1,2]. It is expected that BMSCs can also promote peripheral nerve regeneration.

This study aimed to create a nerve conduit from BMSCs using a Bio-3D printer and to evaluate its potential for nerve regeneration in a rat sciatic nerve model.

[1] Department of Orthopaedic Surgery, Kyoto University Graduate School of Medicine, Kyoto, Japan
[2] Cyfuse Biomedical K.K., Tokyo, Japan
[3] Department of Regenerative Medicine and Biomedical Engineering, Saga University, Saga, Japan
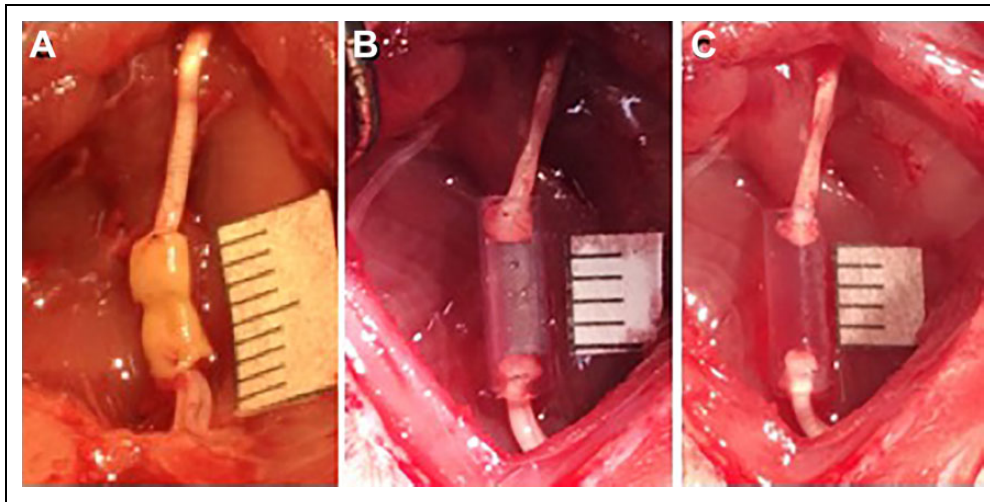
Corresponding Author:
Ryosuke Ikeguchi, Department of Orthopaedic Surgery, Kyoto University Graduate School of Medicine, 54 Shogoin-Kawahara-cho, Sakyo-ku, Kyoto 606-8507, Japan.
Email: ikeguchir@me.com

Figure 1. Five-millimeter gaps in rat sciatic nerves were bridged by conduits of three types. (A) Bio 3D group, (B) S group, and (C) SC group.

Materials and Methods

A total of 20 male Lewis (LEW) rats (8–12 weeks old; 200–300 g, Japan SLC, Inc., Japan) were used. Rats were housed in flat-bottomed cages in pathogen-free rooms with unlimited food and water. All experiments were performed in accordance with the guidelines of the Animal Research Committee, Kyoto University Graduate School of Medicine, Kyoto, Japan.

Generation of BMSCs

BMSCs were isolated from the bone marrow of the femurs and tibias of two LEW rats according to the method of Azizi et al. as in our previous report[11,12]. Briefly, after LEW rats were sacrificed by CO_2 inhalation, bilateral femurs and tibias were extracted. The bone marrow was flushed out by injecting 5 ml of Dulbecco's modified Eagle's medium (DMEM) (Sigma-Aldrich, St. Louis, MO, USA) solution through an 18-gauge needle inserted into the bone and collected in a sterile culture dish. BMSCs were cultured in DMEM containing 10% fetal bovine serum and 1% antibiotic-antimycotic agent (10,000 U/ml penicillin and 10,000 mg/ml streptomycin: Sigma-Aldrich) and incubated at 37°C in an atmosphere of 95% humidity and 5% CO_2. After 48 h incubation, BMSCs were collected from the bottom of the dish. BMSCs were subsequently subcultured four times before being subjected to the experimental procedures. BMSCs were characterized as previously described[12].

Creation of Bio 3D Conduits

Conduits were fabricated from BMSCs using a Bio-3D Printer (Regenova, Cyfuse, Tokyo, Japan) as described by Itoh et al. and Yurie et al.[1,3,13]. Briefly, cells that had been detached and collected by trypsin treatment were centrifuged and resuspended in a minimal volume of new media. An appropriate amount of cell suspension at a concentration of 3×10^5 cells/ml was incubated in a Low Cell Adhesion 96-well plate (SUMILON PrimeSurface, Sumitomo Bakelite, Tokyo, Japan). After 24 h, cells aggregated to form homogeneous multicellular spheroids with diameters of 750 ± 50 μm. To assemble these spheroids into the desired conduits, we used a Bio-3D Printer with the Kenzan method as follows. A robotic system was used to place the spheroids among the skewers of a 9×9 needle array; these spheroids then merged into a three-dimensional cellular structure according to a predesigned 3D model. Approximately 1 week after 3D printing, adjacent spheroids had become fused into a single tubular shape, which we then removed from the Kenzan needle array. Next, the conduit was transferred to a 18-gauge intravenous catheter (SURFLO: NIPRO, Osaka, Japan) perforated with a 22-gauge needle. The spheroids were then cultured in a perfusion bioreactor to promote self-organization of the living cells until the desired function and strength of the tissue was achieved. Each conduit was 8 mm in length with a 2-mm internal diameter and a wall thickness of 500 μm. Bio 3D conduits were evaluated for cell viability immediately before the transplantation using a LIVE/DEAD Viability/Cytotoxicity Kit (Thermo Fisher Scientific K.K., Yokohama, Japan).

Surgical Technique and Experimental Group

Rats were placed under general anesthesia by intraperitoneal injection of sodium pentobarbital (50 mg/kg) and inhalation of isoflurane in oxygen for maintenance. A longitudinal skin incision was made from the right gluteal lesion to the popliteal fossa. The right sciatic nerve of each rat was exposed through a gluteal muscle split and cut in the middle of the thigh to create a 5-mm nerve defect. An 8-mm Bio 3D conduit was interposed into this region, and the proximal and distal nerve stumps were secured 1.5 mm into the tube to bridge the 5-mm interstump gap in the conduit (Bio 3D group, $n = 7$) (Fig. 1). Both proximal and distal nerve stumps

were anchored with 10-0 nylon sutures. The wound was closed in layers with 5-0 nylon sutures. For postoperative analgesia, intraperitoneal fentanyl 0.02 mg/kg was administered. In the silicone group (S group, $n = 5$), a silicone tube 8 mm long with a 2-mm internal diameter was interposed in the same procedure. In the silicone cell group (SC group, $n = 5$), an identical silicone tube 8 mm long with a 2-mm internal diameter was grafted as described above and 4×10^7 BMSCs were immediately injected into this silicone tube with 1 ml phosphate buffer saline. Following their respective procedures, the animals' condition was monitored every day.

Kinematic Analysis

Eight weeks after surgery, we assessed the kinematic properties of the rats' hind limbs while they walked on a treadmill. Prior to the walking session, each rat was equipped with joint markers according to a previously described procedure[14]. Six landmarks for each hind limb were marked using plastic markers or ink. First, colored hemispheric plastic markers were bilaterally attached onto the shaved skin of five upper landmarks: the anterior superior iliac spine, trochanter major joint (hip), knee joint (knee), lateral malleolus (ankle), and fifth metatarsophalangeal joint (MTP). To locate the toe, acrylic resin ink (paint marker, NIPPON-PAINT Co., Ltd, Tokyo, Japan) was applied to the tip of the middle toe. Hind limb motion was captured at a sampling rate of 120 Hz using a 3D motion capture apparatus (Kinema Tracer System, Kissei Comtec, Nagano, Japan) while rats walked at a pace of 10 cm/s. For each rat, a total of 10 steps selected from sequences in which the rat had walked at least five consecutive steps was included in subsequent analysis. Markers were traced, and 3D displacements were reconstructed by the system. For the present study, we analyzed two parameters: (1) drag toe (DT), i.e., the proportion of steps in which the rat's toe did not come off the ground relative to the total number of steps; and (2) angle of attack (AoA), i.e., the angle of the toe to the metatarsal bone at the final segment of the swing phase. A smaller DT value represents less toe dragging. A smaller (sub-zero) AoA value indicates that the toe is placed in plantar flexion immediately before the rat's paw makes contact with the ground.

Electrophysiological Studies

After kinematic analysis, the bilateral sciatic nerves were exposed under general anesthesia and electrophysiological evaluations were performed according to the methods described in our previous report[1]. Briefly, the right sciatic nerve was stimulated just distal to the piriformis muscle (S1) and at the popliteal fossa (S2) using an electromyogram measuring system (Neuropack S1 MEB-9404, NIHON KOHDEN, Tokyo, Japan). Two pairs of needle electrodes were inserted into the pedal adductor muscle to check for the presence of compound muscle action potentials (CMAP) in the muscle. The amplitude (peak to peak) of the CMAP that were evoked in the pedal adductor muscle in response to supramaximal electric stimulation from S1 was measured. The distance between S1 and S2 was measured to calculate the motor nerve conduction velocity (MNCV). The same procedure was performed on the left hind limb. The MNCV and the CMAP in the pedal adductor muscle of the right hind limb were expressed as percentages of those in the left hind limb.

Histological and Morphometric Studies

Eight weeks after surgery, following electrophysiological study, regenerated nerves were removed from in each group, fixed in 1% glutaraldehyde and 1.44% paraformaldehyde, post-fixed with 1% osmic acid, and embedded in epoxy resin. We prepared transverse sections (1 μm thick) from the mid-portion of the regenerated nerves. Sections were stained with 0.5% (w/v) toluidine blue solution and examined under light microscopy (Nikon ECLIPSE 80i, Tokyo, Japan). Total myelinated axon number was counted, and myelinated axon diameter, myelin thickness, and G-ratio were measured using ImageJ software (National Institutes of Health, Bethesda, MD, USA) for morphometric analysis, as reported in our previous studies[1]. Briefly, the total neural area (a) of each specimen was calculated by choosing six or seven fields at random so that the area analyzed would represent >20% of the entire neural area of each specimen. The number of myelinated axons (b), neural area (c), shortest diameter of each myelinated axon (d), and axon diameter (e) were calculated for each field at a final magnification of ×400. The number of myelinated axons and neural areas from all analyzed fields were then summed. The total number of myelinated axons in each specimen was estimated as $b \times (a/c)$. The mean myelinated axon diameter represents the average of the narrowest diameter of each myelinated axon in each of the six or seven fields evaluated. The mean myelin thickness was estimated as $(d - e)/2$ and represents the mean of all myelin thicknesses in the six or seven fields evaluated. Ultrathin sections of the same tissues stained with uranyl acetate and lead citrate were examined under transmission electron microscopy (TEM; Model H-7000; Hitachi High-Technologies, Tokyo, Japan).

Wet Muscle Weight of the Tibialis Anterior Muscle

After removing the regenerated nerve, the bilateral tibialis anterior muscles were dissected and detached from the bone at their origin and insertion, and weighed immediately using a digital scale. The wet muscle weight in the right hind limb was expressed as a percentage of that in the left hind limb.

Immunohistochemistry

Eight weeks after surgery, two rats from the Bio 3D group were sacrificed by means of CO_2 euthanasia for immunohistochemical study. The regenerated peripheral nerves were
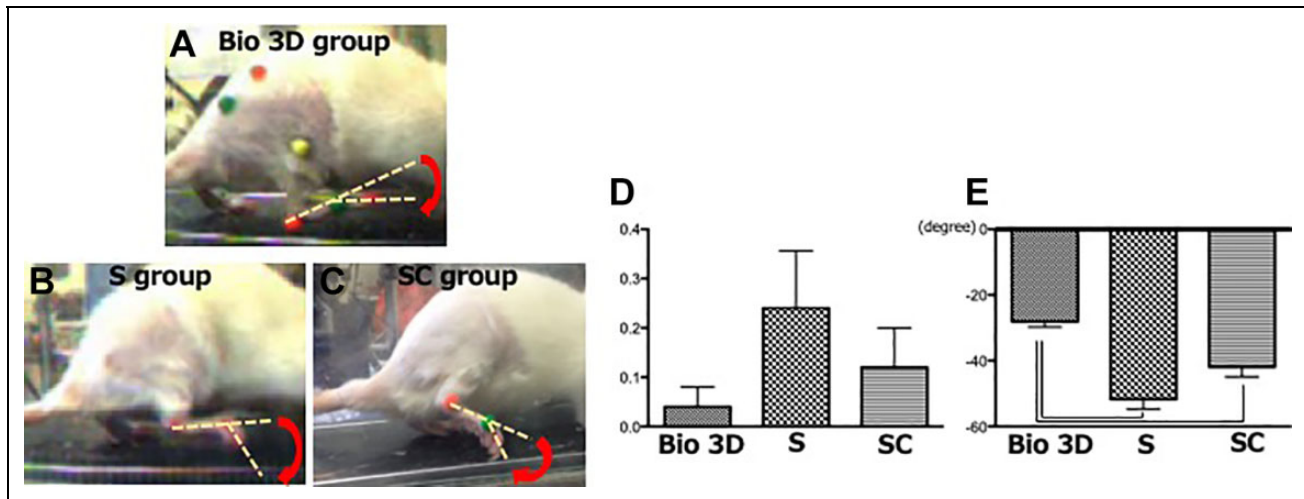
Figure 2. Kinematic study 12 weeks after surgery. (A) AoA, the angle of the toe to the metatarsal bone, in the Bio 3D group. (B) AoA in the S group. (C) AoA in the SC group. (D) DT, the proportion of steps in which the toe does not come off the ground. (E) Comparison of AoA. Brackets indicate significant differences. AoA: angle of attack; DT: drag toe.

exposed and removed. After fixation with 4% paraformaldehyde and cryoprotection with 20% sucrose, cryostat transverse and longitudinal sections (20 μm thickness) were prepared. After rinsing with phosphate-buffered saline (PBS), antigen retrieval was performed using proteinase K (Sigma-Aldrich) at room temperature for 10 min. For blocking, donkey serum was added to the slides, followed by incubation at room temperature for 1 h. Primary antibody was then added, and sections were incubated at 4°C for 24 h. Primary antibodies included rabbit polyclonal anti-S100 protein (S-100) antibody (1:1,000, Dako, Carpinteria, CA, USA) and mouse monoclonal anti-neurofilament H (NF-200) antibody (1:50, Abcam, Tokyo, Japan). Slides were then washed with PBS and incubated with secondary antibody [donkey anti-rabbit IgG (H + L), CFTM543 antibody, Sigma-Aldrich; donkey anti-mouse IgG (H + L), CFTM488 antibody, Sigma-Aldrich] at room temperature for 1 h. After further PBS washing, DAPI (4′,6-diamidino-2-phenylindole, dihydrochloride) solution (1:2,000, DOJINDO, Kumamoto, Japan) was added to the slides. After further PBS washing, cover slips were mounted onto the slides using bicarbonate-buffered glycerol (pH 8.6), and slides were viewed using confocal microscopy (BZ-X700; KEYENCE, Osaka, Japan).

Cell Trafficking Analysis

BMSCs were labeled with PKH26 red fluorescent linker dye (Sigma-Aldrich). The Bio 3D conduit was created from PKH26-labeled BMSCs according to the method described above and transplanted into the nerve gap through an identical surgical procedure. Eight weeks after surgery, the regenerated nerve was removed and immunohistochemical staining was performed as described above with S-100, p75-NTR, and GFAP antibody.

Statistical Analysis

Results are reported as the mean $\pm$ standard error of the mean. Data were compared using analysis of variance. When a significant difference was detected, a post hoc test was applied using the Bonferroni–Dunn method. Differences were considered statistically significant at $P < 0.05$.

Results

Identification of BMSCs and Viability of Bio 3D Conduits

In our phenotypic analysis, flow cytometry results indicated that BMSCs were positive for CD29 and CD90 but negative for CD11b and CD45. Under culture conditions favoring adipogenic, chondrogenic, or osteogenic differentiation, BMSCs differentiated into cells with adipogenic, chondrogenic, or osteogenic phenotypes, respectively (Supplemental Fig. 1). In our LIVE/DEAD viability assay to determine the viability of the Bio 3D conduits, the majority of the cells analyzed were stained green (Supplemental Fig. 2), indicating that they were alive.

Kinematic Analysis

Eight weeks after the surgery, kinematic analysis was performed. The mean DT was 0.04 ± 0.09 in the Bio 3D group, 0.24 ± 0.26 in the S group, and 0.12 ± 0.18 in the SC group (Fig. 2). The mean AoA was -28.1 ± 3.8 in the Bio 3D group, -51.7 ± 6.8 in the S group, and -41.9 ± 6.7 in the SC group. The kinematic study revealed significant differences in AoA between the Bio 3D and silicone groups and between the silicone and silicone cell groups ($P = 0.0001$ and $P = 0.0083$, respectively).
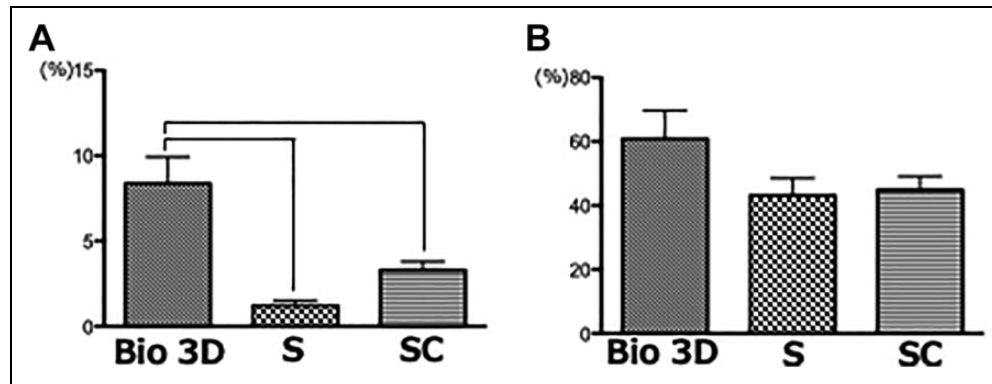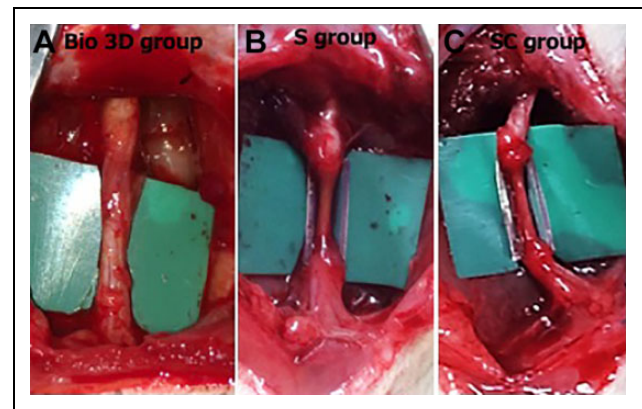
Figure 3. CMAP in the pedal adductor muscles. Brackets indicate significant differences. (A) MNCV in the regenerated nerves. CMAP: compound muscle action potentials; MNCV: motor nerve conduction velocity.

Electrophysiological Studies

The mean CMAP was $8.4 \pm 3.5\%$ in the Bio 3D group, $1.2 \pm 0.7\%$ in the S group, and $3.3 \pm 1.1\%$ in the SC group. The mean MNCV was $60.8 \pm 20.0\%$ in the Bio 3D group, $43.2 \pm 12.1\%$ in the S group, and $44.8 \pm 9.7\%$ in the SC group. The pedal adductor muscle amplitude was significantly different between the Bio 3D and silicone groups ($P = 0.0167$) (Fig. 3).

Macroscopic Observation

Eight weeks after the surgery, nerve gaps had been successfully bridged in all rats in all three groups. In the Bio 3D group, nerve regeneration was confirmed and no neuroma formation was found. In the silicone and silicone cell groups, thin regenerated nerves were observed (Fig. 4).

## Histological and Morphometric Studies

Eight weeks after transplantation, histological study revealed that, in transverse sections of the regenerated nerves, myelinated axons were more abundant in the Bio 3D group than in either of the other two groups (Fig. 5). The total number of myelinated axons was $8{,}446 \pm 408$ in the Bio 3D group, $2{,}968 \pm 743$ in the S group, and $6{,}238 \pm 1{,}075$ in the SC group. These myelinated axon numbers were significantly different among the three groups ($P < 0.01$ in each case). The mean myelinated axon diameter was 2.51 ± 0.34 μm in the Bio 3D group, 2.34 ± 0.32 μm in the S group, and 2.32 ± 0.20 μm in the SC group; this value was not significantly different among the groups. The mean myelin thickness was 0.58 ± 0.06 μm in the Bio 3D group, 0.41 ± 0.08 μm in the S group, and 0.50 ± 0.04 μm in the SC group. Myelin thickness was significantly greater in the Bio 3D group than in the S group ($P < 0.01$).

Figure 4. Macroscopic observation of regenerated nerves. (A) Bio 3D group, (B) S group, and (C) SC group. In the Bio 3D group, thick nerve regeneration is observed.

Wet Muscle Weight of the Tibialis Anterior Muscle

The tibialis anterior muscle showed less muscle atrophy in the Bio 3D group than in either of the control groups (Fig. 6). The proportions of right tibialis anterior muscle weight to left (healthy limb) tibialis anterior muscle weight were $60.0 \pm 13.2\%$ in the Bio 3D group, $32.4 \pm 7.0\%$ in the S group, and $43.7 \pm 4.3\%$ in the SC group. Wet muscle weight was significantly higher in the Bio 3D group than in the silicone group or the silicone cell group ($P < 0.01$ and $P = 0.03$, respectively).

Immunohistochemistry

Eight weeks after the surgery, transverse sections revealed both S-100 and DAPI in all three groups (Fig. 7). S-100- and DAPI-positive cells were abundant in the Bio 3D group, scarce in the silicone group, and intermediate in the silicone cell group. Longitudinal sections revealed both S-100 and NF-200 in all three groups. Tissues from rats in the Bio 3D
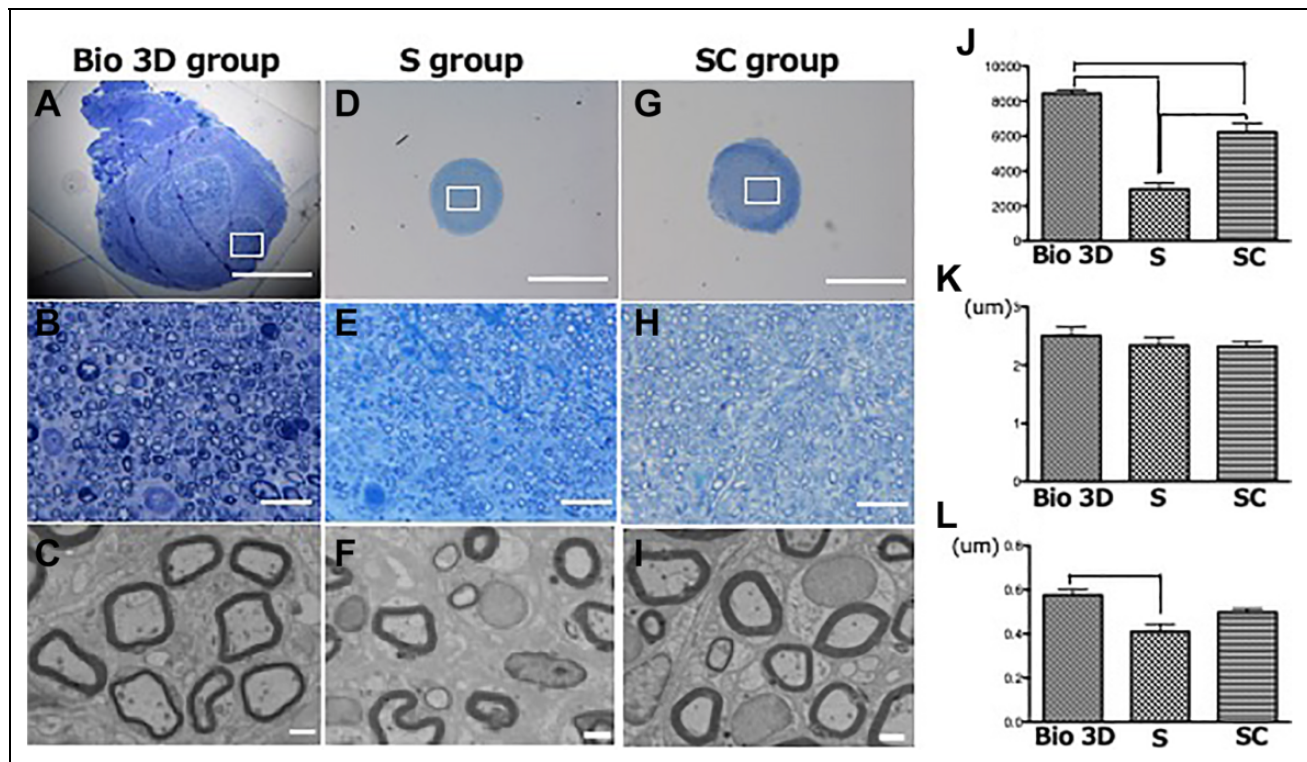
Figure 5. Histological and morphological evaluations. (A) Transverse section of the regenerated nerve in the Bio 3D group. Scale bar = 1,000 μm. The square indicates the area shown in (B). (B) Enlarged image of the area in the square in (A) in the Bio 3D group. Scale bar = 50 μm. (C) Transmission electron microscopic image of the regenerated nerve in the Bio 3D group. Scale bar = 2 μm. (D–F) Images comparable to (A–C) in the S group. (G–I) Images comparable to (A–C) in the SC group. (J) Myelinated axon counts in the three groups. Brackets indicate significant differences. (K) Myelinated axon diameters in the three groups. (L) Myelin thicknesses in the three groups. Brackets indicate significant differences.

group contained many S-100-positive cells and NF-200-positive regenerated axons.

Cell Trafficking Analysis

PKH26-labeled μBMSCs were transplanted. Eight weeks after the transplantation, some of the PKH26-positive cells also expressed the Schwann cell markers S-100, p75-NTR, and GFAP.

Discussion

Autologous nerve graft is considered the gold standard treatment for peripheral nerve injury with interstump gap[15]. Yet harvesting a healthy nerve for this purpose often results in donor site morbidity such as pain and sensory disturbance. To overcome these drawbacks, artificial neural tube implantation has been developed as an alternative to autologous nerve graft. Supporting cells, scaffolds, blood vessels, and growth factors are essential for peripheral nerve regeneration[16], but artificial neural tubes include only scaffolds and so do not enable sufficient nerve regeneration comparable to that achieved through autologous nerve graft. Some researchers have attempted to resolve this problem by adding

certain cell types to the conduit to promote better nerve regeneration[9,17,18]. The survival rate of these injected cells is low, however[19]. To compare different methods of applying these cells, the current study included a silicone cell group in which nerve gaps were filled with silicone injected with MSCs. Through electrophysiological, kinematic, and morphological assessment, we confirmed that nerve regeneration was significantly better in the Bio 3D group than in the silicone cell group.

Since the inner diameter of the silicone tube is 2 mm while the length of the nerve gap is 5 mm, we expected that approximately 0.0157 ml would be a sufficient quantity of liquid to contain the injected cells. Leakage presented a problem, however, and we were not able to estimate the volume of the fluid leaking into the surgical field prior to injection. To overcome any issues arising from leakage, we prepared 1 ml of cell-containing liquid and filled the silicone tube with this liquid during leakage in the silicone cell group. This means that, in the silicone cell group, the amounts of cells applied were smaller than we had intended for this experiment. Therefore, this administration method is not suitable for these cells as it does not lead to sufficient nerve regeneration.
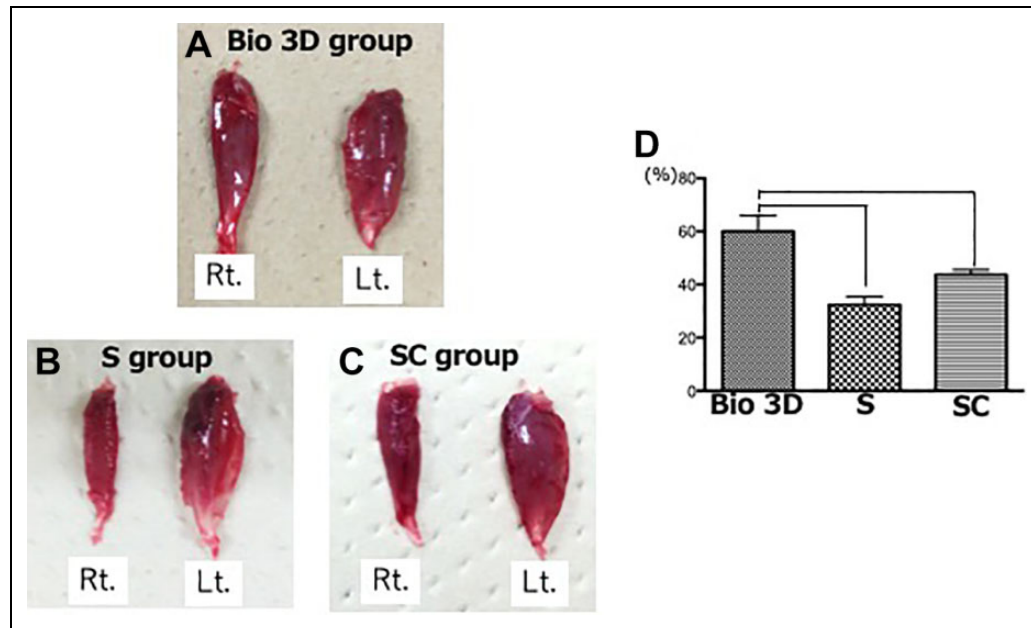
Figure 6. Wet muscle weight of the tibialis anterior muscle. (A) Bilateral tibialis anterior muscles in the Bio 3D group. (B) Bilateral tibialis anterior muscles in the S group. (C) Bilateral tibialis anterior muscles in the SC group. (D) Wet muscle weight of the right tibialis anterior muscle as a proportion of that of the left tibialis anterior muscle. Brackets indicate significant differences.
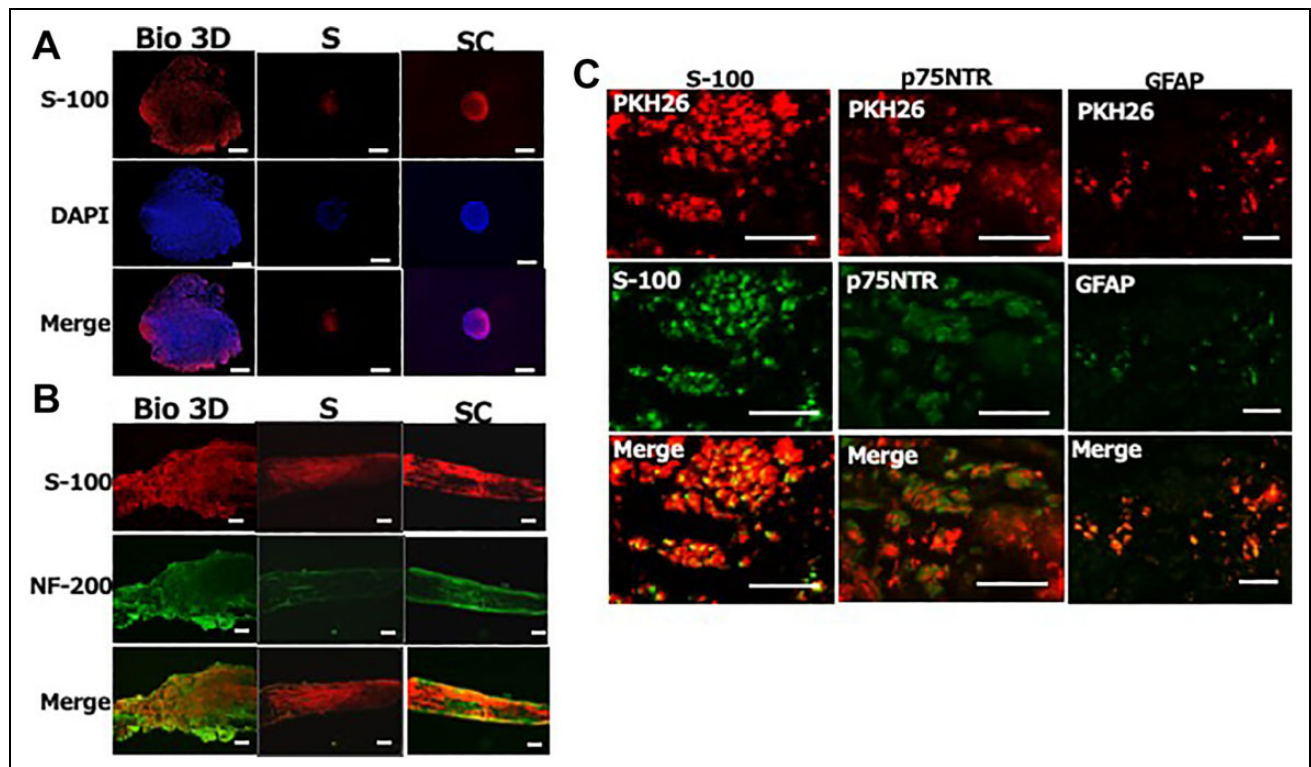
Figure 7. Immunohistochemical staining of regenerated nerves 8 weeks after surgery. (A) S-100 and DAPI staining of transverse nerve sections in the three groups (Bio 3D: Bio 3D group, S: S group, and SC: SC group). The Bio 3D group contains more S-100-positive cells. (B) S-100 and NF-200 staining of longitudinal nerve sections. The Bio 3D group contains more S-100-positive cells and more NF-200-positive neurofilaments. (C) PKH26-labeled cells in cell trafficking analysis. Some PKH26-positive cells were also positive for the Schwann cell markers S-100, p75NTR, and GFAP. DAPI: 4',6-diamidino-2-phenylindole.

In the electrophysiological portion of our study, pedal adductor muscle CMAP was significantly different among the three groups. MNCV, on the other hand, did not differ significantly among the groups. MNCV represents the conduction of large myelinated axons only. At 8 weeks after the surgery, the regenerated nerves included a mixture of small and large myelinated axons because of axon sprouting. At that time, accordingly, significant differences in MNCV are unlikely to be detected.

In the kinematic portion of our study, AoA was significantly different among the three groups. DT, on the other hand, was not significantly different. AoA, which represents the angle of the toe to the metatarsal bone, is a simple evaluation of muscle function in the lower leg and foot. The AoA finding is consistent with our electrophysiological findings regarding CMAP of the pedal adductor muscles. DT, in contrast, is the proportion of steps in which the toe did not come off the ground; this depends not only on the functionality of the operated limb but on the functionality of the entire lower half of the rat's body. Therefore, DT does not represent functional recovery of the regenerated nerves.

We confirmed that transplanted BMSCs differentiated into Schwann cell–like cells. In our cell trafficking analysis, some PKH26-positive cells were also positive for the Schwann cell markers S-100, p75-NTR, and GFAP. It has been reported that BMSCs differentiate into Schwann cell–like cells both *in vitro* and *in vivo*[20,21]. In our study, likewise, transplanted BMSCs differentiated into Schwann cell–like cells. We expect that the regenerated nerves included both differentiated Schwann cell–like cells and migrated Schwann cells from the nerve stumps. This explains why our immunohistochemical study found that the Bio 3D group had more S-100-positive cells in the transverse and longitudinal sections, indicating the existence of more functional Schwann cells, leading to better nerve regeneration in this group than in either of the other two groups.

BMSCs have an advantage to differentiate into Schwann cell–like cells. However, BMSCs have some disadvantages such as invasive bone marrow harvesting and neoplastic transformation. On the other hand, fibroblasts less differentiate into Schwann cell–like cells than BMSCs[22], but they have some advantages of promoting Schwann cell migration[23], less invasive harvest, and easy handling. Further studies are needed.

Conclusion

Our Bio 3D conduit efficiently supports regeneration by providing BMSCs, which then successfully differentiate into Schwann cell–like cells. Our Bio 3D conduit derived from BMSCs promotes peripheral nerve regeneration and should be considered as a treatment option for peripheral nerve surgery.

Author Contributions

Ryosuke Ikeguchi, Tomoki Aoyama, Shizuka Akieda, Koichi Nakayama, and Shuichi Matsuda made contributions to the definition of intellectual content. Hirofumi Yurie, Mai Tanaka, Hiroki Oda, Hisataka Takeuchi, Sadaki Mitsuzawa, Maki Ando, and Koichi Yoshimoto performed the experimental study and data acquisition. Ryosuke Ikeguchi, Tomoki Aoyama, Takashi Noguchi, and Shizuka Akieda analyzed the data. All authors wrote, reviewed, and approved the manuscript.

Ethical Approval

The experimental protocols were approved by the Animal Research Committee, Kyoto University Graduate School of Medicine.

Statement of Human and Animal Rights

All animal studies were approved by the Animal Research Committee, Kyoto University Graduate School of Medicine and were performed according to the guidelines of the Animal Research Committee, Kyoto University Graduate School of Medicine.

Statement of Informed Consent

There are no human subjects in this article and informed consent is not applicable.

Declaration of Conflicting Interests

The author(s) declared the following potential conflicts of interest with respect to the research, authorship, and/or publication of this article: Koichi Nakayama is the co-founder and shareholder of Cyfuse Biomedical K.K., Tokyo, Japan (Cyfuse). Shizuka Akieda, who is the president of Cyfuse, contributed to the manufacturing of 3D conduits and Cyfuse provided the bioprinter to manufacture the conduit. Cyfuse also provided support in the form of a salary for Shizuka Akieda and provided research grants to Ryosuke Ikeguchi, Tomoki Aoyama, Koichi Nakayama, and Shuichi Matsuda. Cyfuse did not have any additional role in the study design, data collection, and analysis; decision to publish; or preparation of the manuscript. These competing interests do not alter the authors' adherence to Cell Transplantation policies on sharing data and materials.

ORCID iDs

Ryosuke Ikeguchi https://orcid.org/0000-0003-4525-7849
Sadaki Mitsuzawa https://orcid.org/0000-0002-6766-5512
Koichi Nakayama https://orcid.org/0000-0002-7324-8862

Supplemental Material

Supplemental material for this article is available online.

References

1. Yurie H, Ikeguchi R, Aoyama T, Kaizawa Y, Tajino J, Ito A, Ohta S, Oda H, Takeuchi H, Akieda S, Tsuji M, et al. The efficacy of a scaffold-free Bio 3D conduit developed from human fibroblasts on peripheral nerve regeneration in a rat sciatic nerve model. PLoS One. 2017;12(2):e0171448.

2. Takeuchi H, Ikeguchi R, Aoyama T, Oda H, Yurie H, Mitsuzawa S, Tanaka M, Ohta S, Akieda S, Miyazaki Y, Nakayama K, et al. A scaffold-free Bio 3D nerve conduit for repair of a 10-mm peripheral nerve defect in the rats. Microsurgery. 2020; 40(2):207–216.

3. Murata D, Arai K, Nakayama K. Scaffold-free Bio-3D printing using spheroids as 'Bio-inks' for tissue (Re-)construction and drug response tests. Adv Healthc Mater. 2020;e1901831.

4. Arai K, Murata D, Takao S, Verissiomo A, Nakayama K. Cryopreservation method for spheroids and fabrication of scaffold-free tubular constructs. PLoS One. 2020;15(4): e0230428.

5. Taniguchi D, Matsumoto K, Machino R, Takeoka Y, Elgalad A, Taura Y, Oyama S, Tetsuo T, Moriyama M, Takagi K, Kunizaki M, et al. Human lung microvascular endothelial cells as potential alternatives to human umbilical vein endothelial cells in bio-3D-printed trachea-like structures. Tissue Cell. 2020;63:101321.

6. Itoh M, Mukae Y, Kitsuka T, Arai K, Nakamura A, Uchihashi K, Toda S, Matsubayashi K, Oyama J, Node K, Kami D, et al. Development of an immunodeficient pig model allowing long-term accommodation of artificial human vascular tubes. Nat Commun. 2019;10(1):2244.

7. Nakanishi Y, Okada T, Takeuchi N, Kozono N, Senjyu T, Nakayama K, Nakashima Y. Histological evaluation of tendon formation using a scaffold-free three-dimensional-bioprinted construct of human dermal fibroblasts under *in vitro* static tensile culture. Regen Ther. 2019;11:47–55.

8. Cuevas P, Carceller F, Dujovny M, Garcia-Gómez I, Cuevas B, González-Corrochano R, Diaz-González D, Reimers D. Peripheral nerve regeneration by bone marrow stromal cells. Neurol Res. 2002;24(7):634–638.

9. Yamakawa T, Kakinoki R, Ikeguchi R, Nakayama K, Morimoto Y, Nakamaura T. Nerve regeneration promoted in a tube with vascularity containing bone marrow-derived cells. Cell Transplant. 2007;16(8):811–822.

10. Kaizawa Y, Kakinoki R, Ikeguchi R, Ohta S, Noguchi T, Takeuchi H, Oda H, Yurie H, Matsuda S. A Nerve conduit containing a vascular bundle and implanted with bone marrow stromal cells and decellularized allogenic nerve matrix. Cell Transplant. 2017;26(2):215–228.

11. Azizi SA, Stokes D, Augelli BJ, DiGirolamo C, Prockop DJ. Engraftment and migration of human bone marrow stromal cells implanted in the brains of albino rats–similarities to astrocyte grafts. Proc Natl Acad Sci U S A. 1998;95(7):3908–3913.

12. Ikeguchi R, Kakinoki R, Ohta S, Oda H, Yurie H, Kaizawa Y, Mitsui H, Aoyama T, Toguchida J, Matsuda S. Recipient bone marrow-derived stromal cells prolong graft survival in a rat hind limb allotransplantation model. Microsurgery. 2017; 37(6):632–640.

13. Itoh M, Nakayama K, Noguchi R, Kamohara K, Furukawa K, Uchihashi K, Toda S, Oyama J, Node K, Morita S. Scaffold-free tubular tissues created by a Bio-3D printer undergo remodeling and endothelialization when implanted in rat aortae. PLoS One. 2015;10(9):e0136681.

14. Tajino J, Ito A, Nagai M, Zhang X, Yamaguchi S, Iijima H, Aoyama T, Kuroki H. Intermittent application of hypergravity by centrifugation attenuates disruption of rat gait induced by 2 weeks of simulated microgravity. Behav Brain Res. 2015;287: 276–284.

15. Lundborg G. A 25-year perspective of peripheral nerve surgery: evolving neuroscientific concepts and clinical significance. J Hand Surg Am. 2000;25(3):391–414.

16. Widgerow AD, Salibian AA, Kohan E, Sartiniferreira T, Afzel H, Tham T, Evans GR. Strategic sequences in adipose-derived stem cell nerve regeneration. Microsurgery. 2014;34(4): 324–330.

17. Siemionow M, Duggan W, Brzezicki G, Klimczak A, Grykien C, Gatherwright J, Nair D. Peripheral nerve defect repair with epineural tubes supported with bone marrow stromal cells: a preliminary report. Ann Plast Surg. 2011; 67(1):73–84.

18. Jesuraj NJ, Santosa KB, Newton P, Liu Z, Hunter DA, Mackinnon SE, Sakiyama-Elbert SE, Johnson PJ. A systematic evaluation of Schwann cell injection into acellular cold-preserved nerve grafts. J Neurosci Methods. 2011;197(2):209–215.

19. Walsh SK, Kumar R, Grochmal JK, Kemp SWP, Forden J, Midha R. Fate of stem cell transplants in peripheral nerves. Stem Cell Res. 2012;8(2):226–238.

20. Kashani IR, Golipoor Z, Akbari M, Mahmoudi R, Azari S, Shirazi R, Bayat M, Ghasemi S. Schwann-like cell differentiation from rat bone marrow stem cells. Arch Med Sci. 2011; 7(1):45–52.

21. Chen X, Wang XD, Chen G, Lin WW, Yao J, Gu XS. Study of *in vivo* differentiation of rat bone marrow stromal cells into Schwann cell-like cells. Microsurgery. 2006;26(2):111–115.

22. Thoma EC, Merkl C, Heckel T, Haab R, Knoflach F, Nowaczyk C, Flint N, Jagasia R, Jensen Zoffmann S, Truong HH, Petitjean P, et al. Chemical conversion of human fibroblasts into functional Schwann cells. Stem Cell Rep. 2014;3(4): 539–547.

23. Parrinello S, Napoli I, Ribeiro S, Wingfield Digby P, Fedorova M, Parkinson DB, Doddrell RD, Nakayama M, Adams RH, Lloyd AC. EphB signaling directs peripheral nerve regeneration through Sox-2-dependent Schwann cell sorting. Cell. 2010;143(1):145–155.